Journal of Engineering Mathematics **28**: 1–19, 1994.

On the Propagation of Naturally-Occurring Turbulent Spots

J.P. CLARK, T.V. JONES[1], and J.E. LaGRAFF[2]
[1]*Oxford University, Oxford, U.K.*
[2]*Syracuse University, Syracuse NY, U.S.A.*

Received 3 February 1993; accepted in revised form 13 August 1993

Abstract. An experimental investigation of the propagation of turbulent spots occurring naturally during boundary-layer transition was conducted. Wide-bandwidth heat-transfer instrumentation was used in tracking individual turbulent spots as they progressed down a flat-plate surface toward fully-developed turbulence. The convection rates of the turbulent/non-turbulent interfaces of the spots in the streamwise direction were determined, as were rates of lateral spreading. The separate effects of compressibility and favourable pressure gradients have been assessed, and some typical results have been reported.

List of symbols

C_{le}, *C_le*	fractional propagation rate of the spot leading edge, U_{le}/U_∞
C_m, *C_m*	fractional propagation rate of the spot ("mean"), U_m/U_∞
C_{te}, *C_te*	fractional propagation rate of the spot trailing edge, U_{te}/U_∞
Cr	criterion function
D	detector function
dx	distance of propagation of the lateral edge of a turbulent spot in the streamwise direction (mm)
dz	distance of propagation of the lateral edge of a turbulent spot in the cross-stream direction (mm)
h	sampling period (s)
K	acceleration parameter, $(\nu/U_\infty^2)dU_\infty/dx$
m	relative signal magnitude
M_∞	freestream Mach number
n	turbulent-spot generation rate ($s^{-1}\,m^{-1}$)
P	freestream static pressure (N/m^2)
P_0	total pressure (N/m^2)
q	heat flux (kW/m^2)
Re_u	freestream unit Reynolds number at the working-section inlet (m^{-1}), U_∞/ν
Re_θ	local Reynolds number based on momentum thickness, $U_\infty\theta/\nu$
T_0	total temperature (K)
T_w	wall temperature (K)
Tu	freestream turbulence intensity, u'/U_∞
t_{NT}	amount of time an unsteady heat-transfer signal is non-turbulent (s)
t_T	amount of time an unsteady heat-transfer signal is turbulent (s)
U_{le}	turbulent-spot leading-edge velocity (m/s)
U_m	turbulent-spot "mean" velocity (m/s)
U_{te}	turbulent-spot trailing velocity (m/s)
U_∞	local freestream velocity (m/s)
w	weighting factor
x	distance from the leading edge of the flat plate (m)
x_t	distance from the leading edge of the flat plate to the point of transition onset (m)
α	turbulent-spot spreading angle (degrees)
γ	intermittency, $t_T/(t_T + t_{NT})$
θ	boundary-layer momentum thickness (m)
ν	kinematic viscosity (m^2/s)
σ	Emmons' non-dimensional turbulent-spot propagation parameter
τ_s	smoothing period (s)

Introduction

In 1951, H.W. Emmons [1] of Harvard University, discovered turbulent spots in a water table he had been intending to use for an undergraduate demonstration. This observation led him to formulate the theory that transition to turbulence in boundary layer flows occurs through the formation and growth of individual turbulent regions which eventually coalesce into a fully-turbulent boundary layer. Since this breakthrough in the understanding of the transition process, which has become generally accepted, much work has been devoted to the study of turbulent spots. A detailed synopsis of current knowledge regarding turbulent spots is given by Riley and Gad-el-Hak [2].

Many of the essential features of Emmons' theory were first confirmed by Schubauer and Klebanoff [3], who were also the first to chart the growth and shape of a turbulent spot in three dimensions. Using hot-wire anemometry in air at very low speeds, they found that a turbulent spot resembles an arrowhead in planform. They measured the convection speed of the leading interface of the spot and found that it propagated at 88% of the local freestream velocity. The trailing edge of the spot convected at one half the freestream velocity. Also, they found that, after a brief period of non-linear growth in the spanwise direction, the spot spread laterally in a linear fashion, making an angle of roughly 11° with the freestream. The elevation view of the turbulent spot is characterised by an overhanging lip and a hump in its mid-section. Schubauer and Klebanoff [3] noted that, as the spot travelled downstream, the hump grew as the thickness of a fully-turbulent boundary layer having an initial thickness equal to that of the laminar boundary layer at the point of inception of the spot. This notion was later confirmed by Savas [4] who showed, albeit over a limit range, that an artificially-induced turbulent spot in an otherwise laminar boundary layer grew in the direction normal to the surface as the distance from its origin to the four-fifths power.

Since the landmark experiments of Schubauer and Klebanoff [3], their work has been both confirmed and extended by several other researchers. In particular, Cantwell et al. [5] studied the flow structure and rates of entrainment along the plane of symmetry of an artificially-produced turbulent spot using laser-doppler anemometry in a water tunnel. They concluded that, in an ensemble-averaged sense, the spot consists of two coherent vortex structures. Also, Wygnanski et al. [6] used hot-wire anemometry to map the variation of all three components of velocity inside a turbulent spot along its plane of symmetry. A notable finding of their work was that the streamwise component of velocity increased as the leading interface of the spot passed the fixed probe, and continued to do so throughout the length of the spot. This implied that the magnitude of the surface shear stress also increased along the length of the spot. Later, this hypothesis was verified by Mautner and Van Atta [7], who made direct measurements of the wall shear stress along the plane of symmetry of a turbulent spot using hot-film gauges.

In addition to the above investigations, which all consisted of measurements in constant velocity flow, a few other studies have been conducted to assess the effect of favourable pressure gradients on the transitional spot. The first such study was conducted by Wygnanski [8] who determined that, in a favourable pressure gradient, neither the leading nor the trailing-edge convection rate of the turbulent spot scaled directly with the freestream velocity. This result was later expanded upon by Katz et al. [9], who studied a turbulent spot developing in a boundary layer accelerating in a pressure gradient which could be described by the Falkner-Skan parameter $\beta = 1$. They showed that, under these conditions, the leading- and trailing-edge convection velocities of the spot increased as the square root of

distance from the spot origin, while the freestream velocity increased linearly with the same length. In contrast with the findings of these two studies, Sankaran and Antonia [10] found that, within the uncertainty of their measurements, the leading-edge convection rate of the spot did scale with the freestream velocity in a favourable pressure gradient. However, the trailing-edge convection rate (as a fraction of the local freestream velocity) was seen to increase over the accepted zero pressure gradient value.

One conclusion that all three of the above studies share in common is that the streamwise and spanwise growth rates of turbulent spots are inhibited by a favourable pressure gradient. These results support certain conclusions drawn from flow-visualization experiments by Gad-el-Hak et al. [11] and Matsui [12]. Gad-el-Hak et al. [11] argued that the spot grows in the spanwise direction by the local destabilization of the rotational flow in the ambient laminar boundary layer adjacent to it. The authors pointed out that this is different from the classical definition of entrainment, which concerns the incorporation of non-rotational fluid from the mainstream into the boundary layer. Matsui [12] concluded that the discrepancy between the leading- and trailing-edge convection rates of a turbulent spot was a consequence of the accretion of vortices near the trailing-edge of the spot. It seems plausible that both of these mechanisms for spot growth would be inhibited by the stabilizing influence of a favourable pressure gradient.

The present study is one in a series of transition experiments conducted at Oxford University. The first inquiry into transition at Oxford stemmed from the pioneering work of Schultz and Bellhouse [13] concerning surface-mounted hot-film gauges, and was conducted by Owen [14] on a flat plate at subsonic and supersonic speeds. These investigations established the usefulness of such non-intrusive sensors for the examination of intermittent flows. Following this work, Doorly et al. [15] and LaGraff et al. [16], studied the end-stage of the transition process on a gas-turbine blade in a two-dimensional cascade. Typical results of the work of LaGraff et al. [16] are found in Figure 1, which is an illustration of the unsteady character of transition in a wake-disturbed environment.

The results of LaGraff et al. [16] and Doorly et al. [15] referred to above employed

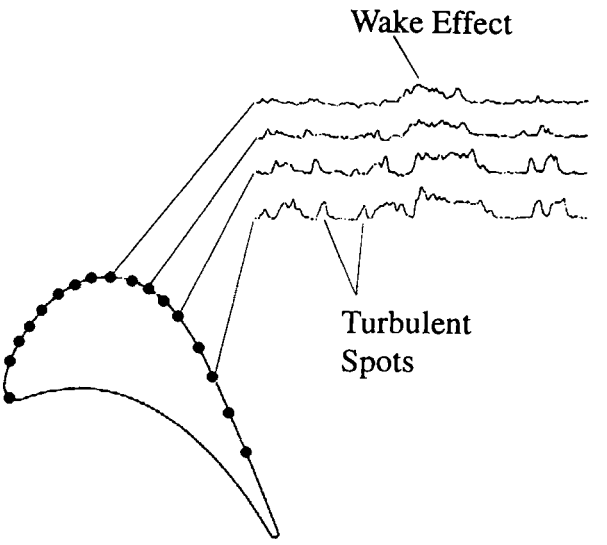

Fig. 1. Typical results from the work of LaGraff et al. [16] illustrating the unsteady nature of transition in a wake-disturbed environment.

"passive" thin-film gauges where the sensor is used as a resistance thermometer to monitor the transient temperature-variation of the model when subjected to a sudden onset of hot flow. Gauges of similar construction may also be utilised as hot films in an unheated steady flow. In the latter case, a high current is passed through the film giving sensible ohmic heating to the gauge and heat transfer to the flow. The rate of heat transfer may be determined by incorporating the hot-film gauge in a constant-temperature-anemometer circuit which outputs a signal proportional to the fluctuating heat-transfer rate. The frequency-response limit of the hot-film gauge is approximately 40 kHz, whereas that of thin-film gauge is greater by a factor of 10. An added advantage of the thin-film heat-transfer gauge is that accurate values of local surface-heat-flux are obtained. Nevertheless, hot-film gauges may also be used to detect turbulent spots and evaluate their properties. As an example, Figure 2 is a set of hot-film signals acquired on the external surface of a turbofan nacelle in flight trials. These trials were part of a European engine-flight-test programme

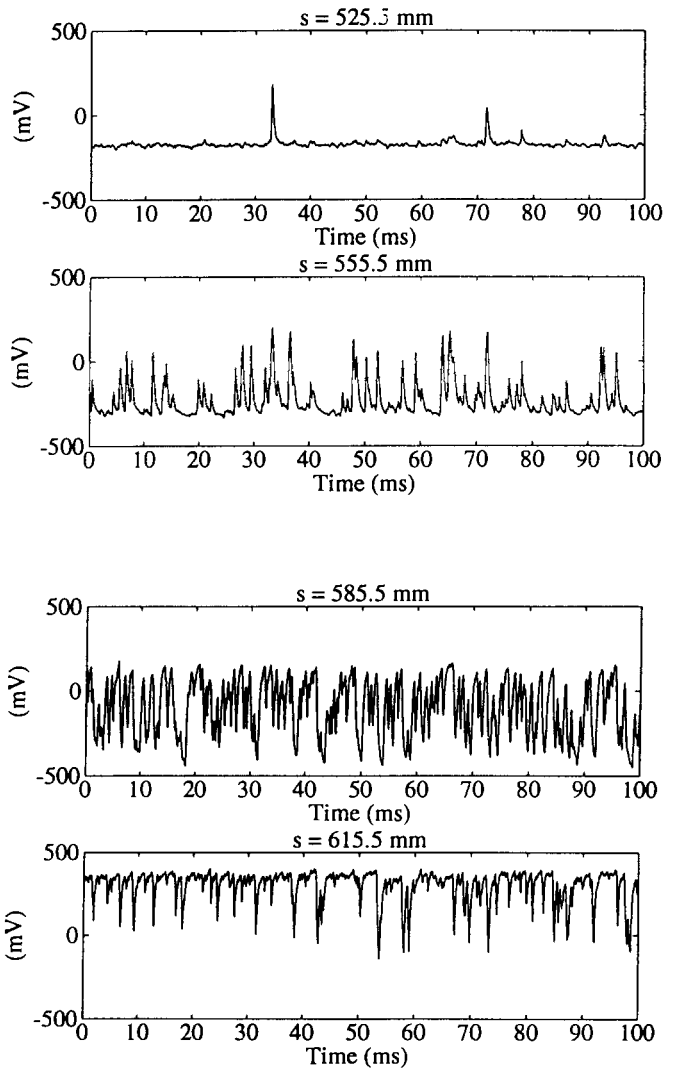

Fig. 2. Unsteady hot-film signals from four locations on the surface of a turbofan nacelle in free flight (from Ref. 17–18).

[17], and the instrumentation was manufactured by the Oxford University turbomachinery group [18] in the same manner as the thin-film gauges used in the experiments reported here. Thus, the two examples of the turbine blade and the jet-engine nacelle demonstrate the universal nature of turbulent-spot phenomena and the range of applications of thin-film gauges.

All of the more fundamental experimental studies described above [2–12] have focused on artificially-generated single turbulent spots in otherwise laminar boundary layers. This experiment goes some way toward bridging the gap between such investigations and the more applied studies of the type undertaken previously at Oxford [13–18]. It extends much of the same information garnered from artificial turbulent-spot investigations to spots occurring naturally, especially at conditions representative of the gas-turbine environment. Edge velocities and spreading angles of naturally-occurring events are determined over a range of Mach numbers and pressure gradients typically encountered on the suction surfaces of gas-turbine blades. Consequently, turbulent spots have been tracked at values of the acceleration parameter approaching the relaminarization limit and at Mach numbers as much as two orders of magnitude greater than those reported elsewhere [2–12].

Description of facility and experimental technique

The present experiments were conducted in the Oxford University 6 inch Isentropic Light-Piston Tunnel (ILPT), which has been described thoroughly by Jones et al. [19]. The ILPT is a transient facility which is capable of producing flows with a range of Reynolds numbers, Mach numbers, and gas-to-wall temperature ratios in order to simulate conditions in modern gas-turbine engines. A schematic of the tunnel is shown in Figure 3. Its major components are the high-pressure reservoir, the pump tube fitted with a light-weight piston, the working section, and a dump tank. During a tunnel run, air is suddenly injected into the pump tube from the high-pressure reservoir through a series of ball valves. This forces the piston down the pump tube from the reservoir end. This action compresses the air ahead of the piston isentropically and thus increases the gas temperature. When the gas in the tube reaches the required conditions, the fast-acting gate valve is opened and the air flows through the test section and into the dump tank in a total running time of roughly 300 ms. If the volumetric flow-rate into the pump tube from the reservoir equals that flowing out through the test section, the total pressure and temperature during the run remain constant, and the run is said to be matched.

During the study, the working section of the ILPT was fitted with a flat plate model and boundary-layer bleed apparatus, as shown schematically in Figure 4. The wall of the test

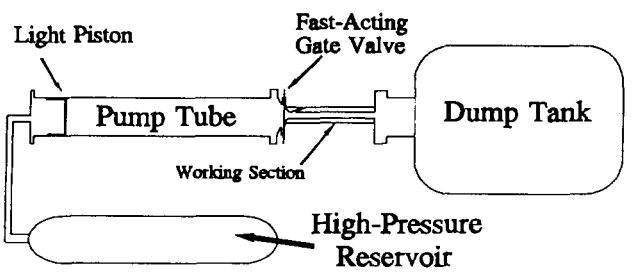

Fig. 3. Schematic of the Isentropic Light-Piston tunnel.

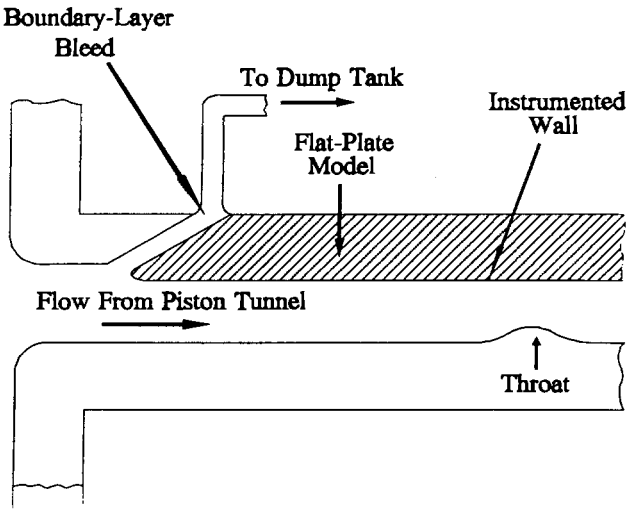

Fig. 4. Schematic of the **ILPT** test section fitted with an instrumented flat plate (subsonic configuration).

section opposite the flat plate was readily removable and a series of convergent-divergent nozzles were available to achieve different constant Mach number flows and pressure gradients over the surface of the plate. The flat plate was instrumented with a large array of thin-film heat-transfer gauges to measure the unsteady heat-flux along the surface of the model. Throughout the course of the study, two flat plates were used. The first was composed of a machinable glass ceramic called Macor and was instrumented with 39 platinum thin-film gauges. These sensors were produced via a painting-and-firing technique. The second plate, which can be seen in Figure 5, was made of perspex and was instrumented with nickel thin-film gauges which were fabricated with an RF-magnetron sputtering technique [20]. The data presented here were obtained with both types of flat plate.

The use of thin-film gauges for the measurement of steady and unsteady heat-fluxes is described in detail by Schultz and Jones [21]. The thin-film gauges used in this study were operated at a constant current, and the signals from the gauges were processed through

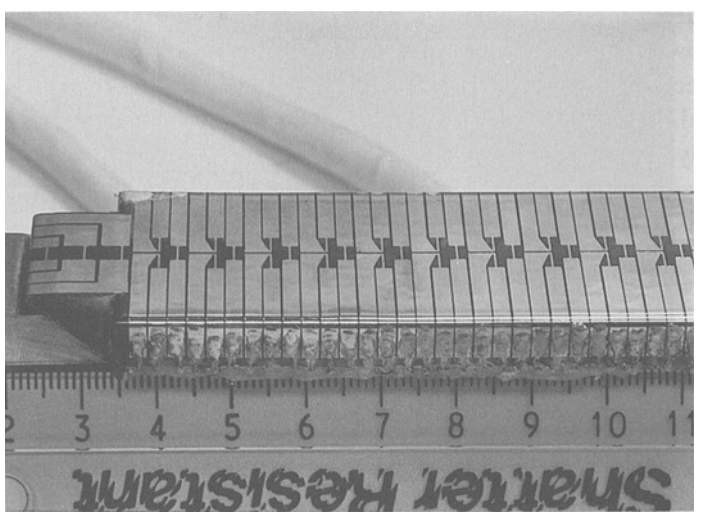

Fig. 5. Photograph of a flat plate instrumented with nickel thin-film gauges. The leading edge of the plate is at left.

electrical analogues of the one-dimensional unsteady heat-conduction equation. The analogues used are based on the design of Oldfield et al. [22] and have a nominal bandwidth of 0.01–100 kHz. High-speed data-acquisition channels are available to monitor 28 thin-film signals simultaneously. Each channel has a maximum data-rate of 1 MHz and a storage capacity of 64 Kb.

It is the unique combination of the ILPT, wide-bandwidth instrumentation, and a modern, high-speed data-acquisition system which makes the study possible. As a turbulent-spot passes over a thin-film gauge, it instantaneously raises the heat-flux at the sensor from the quiet laminar level to a value closer to the turbulent level. Simultaneous sampling of the heat-flux signal at a number of locations on the flat-plate surface enables one to track turbulent spots as they proceed down the model surface. This can be readily seen by inspection of Figure 6, which is a set of four unsteady heat-flux traces from various locations on the flat plate. Obviously, such signals contain a wealth of information regarding the

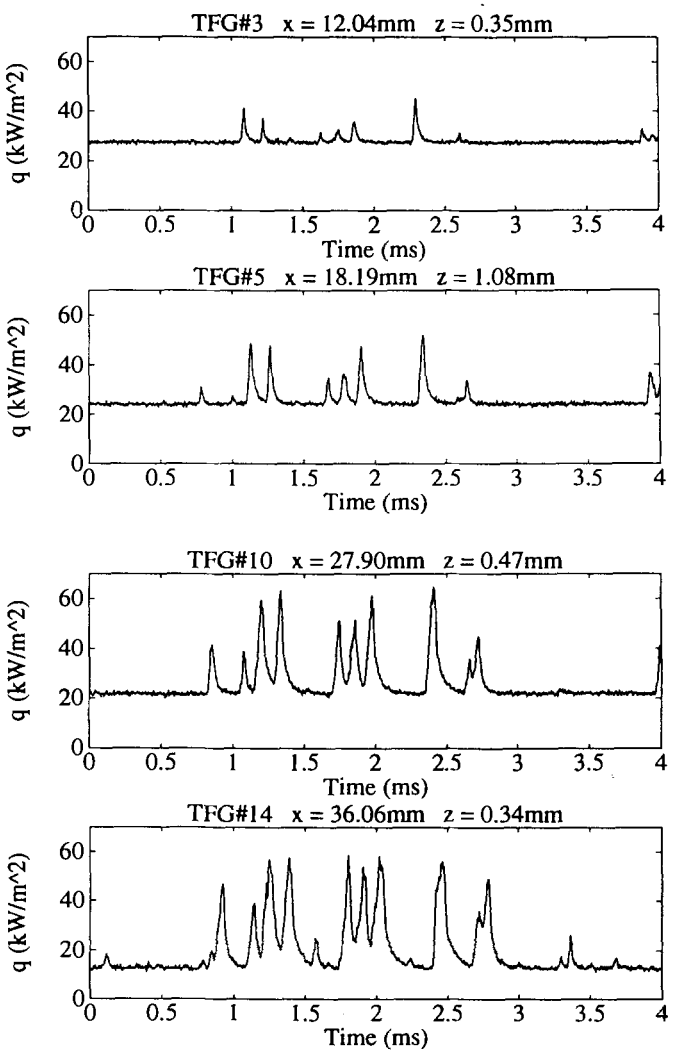

Fig. 6. Unsteady heat-flux traces from four locations on the flat-plate model surface ($M_\infty = 0.55$, $dP/dx = 0$, $Re_u = 7.5 \times 10^6/m$, $Tu = 0.1\%$, and $T_0/T_w = 1.4$) where x is streamwise position and z is spanwise position.

propagation of turbulent spots. Once acquired, such data must then be carefully analyzed to extract turbulent-spot growth parameters.

Analysis techniques

The parameter which best describes the development of transition from a laminar boundary layer toward fully-developed turbulence is the intermittency at the surface. The variation of the intermittency through the transition zone is dictated by the rates of turbulent-spot generation, convection, and lateral spreading. This is apparent from the equation of Narasimha [23]

$$\gamma(x) = 1 - \exp\left\{\frac{-(x - x_t)^2 n\sigma}{U_\infty}\right\}, \tag{1}$$

which results from the application of Emmons' [1] transition model with the assumption of concentrated breakdown in a flat plate, zero-pressure-gradient flow. In Equation 1, x_t is the location of breakdown, n is the number of turbulent spots formed there per unit time and spanwise distance, U_∞ is the freestream velocity, and x is a location on the surface further downstream than x_t. σ is Emmons' [1] non-dimensional spot-propagation parameter, which is dependent upon the convection velocity of the spots and their rate of lateral spreading. In the present study, turbulent-spot convection rates were extracted from raw heat-transfer traces via a digital intermittency detector, while the lateral spreading rate was calculated through estimates of the rate-of-change of thin-film gauge coverage with streamwise distance.

Intermittency detectors, either analog or digital, have been used for a number of years in the analysis of hot-wire signals. A comprehensive review of the technique was given by Hedley and Keffer [24]. In essence, a raw signal is transformed in such a way that a decision for or against the presence of turbulence over the sensor at any given time can be rationally made. Typically, the signal is differentiated and squared to emphasize the high-frequency components it contains. The purpose behind the signal transformation employed by an intermittency detector is to significantly reduce the probability of making an incorrect turbulent/non-turbulent decision over that which would occur if the signal level alone were used as an indicator of turbulent activity.

The process by which turbulent/non-turbulent decisions were made in this study is illustrated in Figure 7. The top trace in Figure 7 is the raw heat-flux signal. The second trace from the top is the detector function (using the terminology of Hedley and Keffer [24]). In this case, the detector function, D_i, is defined as

$$D_i = m\dot{q}_i', \tag{2}$$

where m is the relative magnitude of the signal, given by

$$m = \frac{\dot{q}_i - \dot{q}_{\min}}{\dot{q}_{\max} - \dot{q}_{\min}}, \tag{3}$$

and the first derivative of the instantaneous heat flux is found by the central difference equation

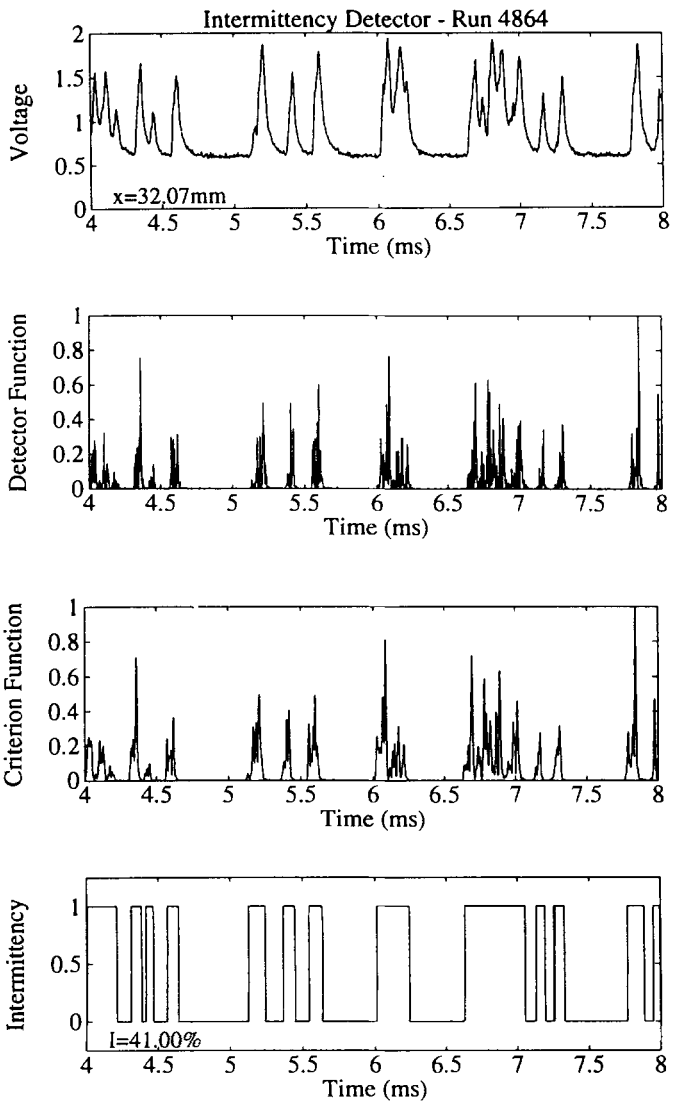

Fig. 7. Transformation of a raw heat-flux signal into an intermittency indicator-function.

$$\dot{q}' = \frac{\dot{q}_{i+1} - \dot{q}_{i-1}}{2h}, \tag{4}$$

where h is the sampling period. The third trace is the criterion function, Cr_i. It is an exponentially-weighted, centred moving-average of the detector function, which is represented by

$$Cr_i = \frac{h^2}{1 + (\tau_s/h)} \sum_{j=i-(\tau_s/2h)}^{j=i+(\tau_s/2h)} w_j D_j, \tag{5}$$

where w_j is the weighting factor, defined by

$$w_j = \exp\{-[0.625/(\tau_s/h)]|j-1|\}\,, \tag{6}$$

and τ_s is the smoothing period. The smoothing period in this case was chosen to be 10μs. This value ensured that the smallest detectable turbulent spots (based on the upper limit of the bandwidth of the instrumentation) were included in the analysis. The bottom trace in Figure 7 is the intermittency signal, or indicator function, which is obtained by setting an appropriate threshold for the criterion function.

The results of the intermittency-detection process can be used to determine the celerities of the leading- and trailing interfaces of the spots as well as the overall intermittency of the flow at a given sensor location. The procedure locates the positions of the spot leading- and trailing edges in time over the thin-film gauges. It is thus possible to determine the trajectories of the turbulent/non-turbulent interfaces of individual spots in the x-t plane. These may be calculated for a number of events and the results processed to produce the trajectories of an "average" spot.

A thin-film gauge has the property of integrating the instantaneous heat-transfer distribution over its sensing area. Consequently, it is possible to make estimates of turbulent-spot lateral growth from the rate-of-change of thin-film-gauge coverage with distance along the model surface. Figure 8 is an illustration of this process. It can be seen that the turbulent spot labelled A in the figure brings the instantaneous heat flux to a value somewhere between the laminar and fully-turbulent levels as indicated on the upper trace of Figure 8. This is because only a fraction of the total gauge-length is covered by the spot. However, as the spot travels downstream it is continually growing in the cross-stream direction. As a result, the spot covers a greater percentage of the gauge represented by the signal plotted in the bottom half of the figure. Knowing the locations of the gauges on the plate, it is possible to determine the position of the lateral edge of the turbulent spot over each gauge. The turbulent-spot spreading angle can then be determined from simple geometry.

Several assumptions are critical to the above analysis. First, the spots are assumed to be triangular in planform. This is a crude assumption in zero pressure gradient flow, but is close

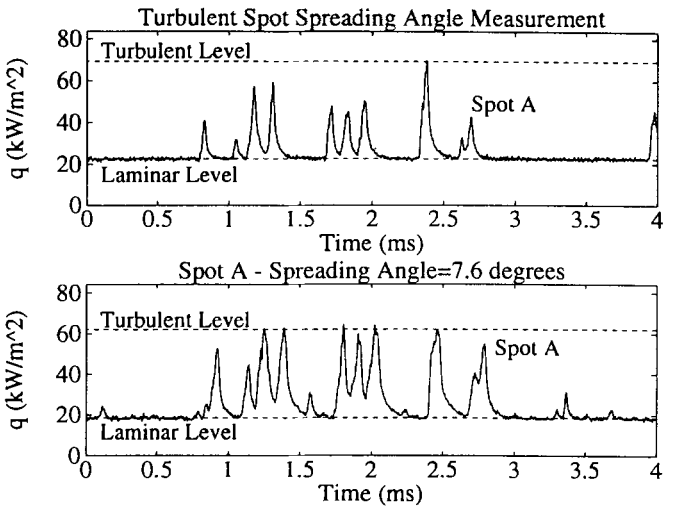

Fig. 8. Turbulent-spot spreading-angle measurement. The streamwise separation between the gauges is 11.95*mm*. The conditions of the run are $M_\infty = 0.55$, $dP/dx = 0$, $Re_u = 7.5 \times 10^6/m$, $Tu = 0.1\%$, and $T_0/T_w = 1.4$.

to the truth for favourable pressure gradients (as detailed by Katz et al. [9]). This first assumption leads directly to the second, where the peak heat flux encountered by the thin-film gauges is assumed to correspond to the passage of the trailing edge of the spot over the gauge. This conjecture is supported by the character of the unsteady traces of Figure 6, as well as the results of Mautner and Van Atta [7] which were mentioned previously. Moreover, Clark et al. [25] showed that in constant-velocity flow the maximum heat-flux levels associated with a given trace were in excellent agreement with the predicted levels for a fully-turbulent boundary layer at the location of the thin-film gauge (the origin of the turbulent boundary layer taken as that location where turbulent spots are first detected). Also, the direction in which the spot is spreading over the thin-film gauges is assumed to be known. In order to determine this, one must measure the instantaneous heat-flux at more than a single spanwise location for at least some streamwise positions. The method by which the direction of spot lateral-propagation is determined can be seen in Figures 9a and 9b. Figure 9a is a set of three unsteady heat-flux traces recorded from three thin-film gauges which are represented schematically in Figure 9b. The top two traces of Figure 9a represent data recorded from the two gauges located at the same streamwise location in Figure 9b. The third trace of Figure 9a contains data from the thin-film gauge which is shown further downstream than the others in Figure 9b. Clearly, the characteristics of the heat-flux traces of Figure 9a could only result from turbulent spots spreading over the thin-film gauges in the same fashion as the spot depicted in Figure 9b is propagating over the three hypothetical gauges.

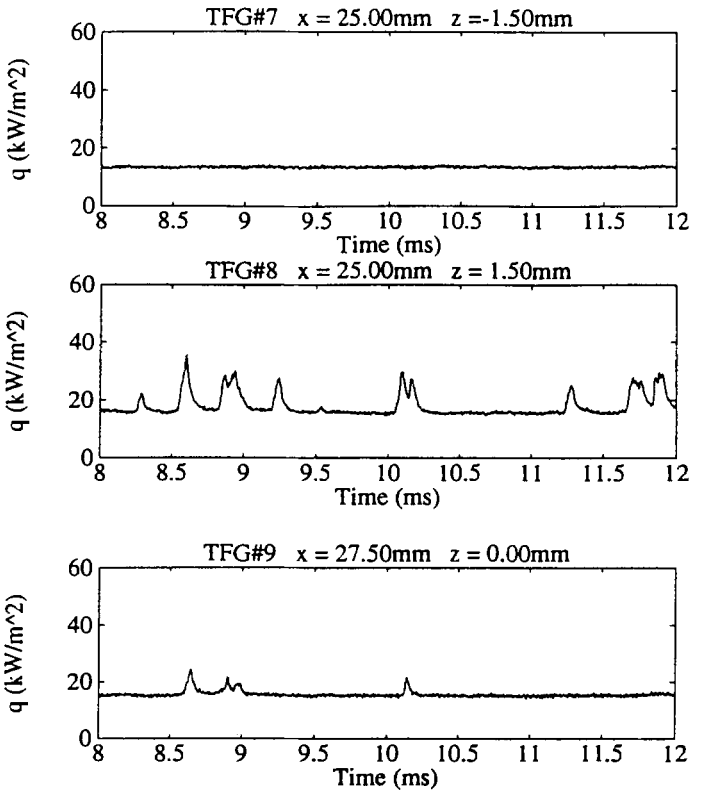

Fig. 9(a). The determination of the direction of turbulent-spot spreading from unsteady heat-flux traces.

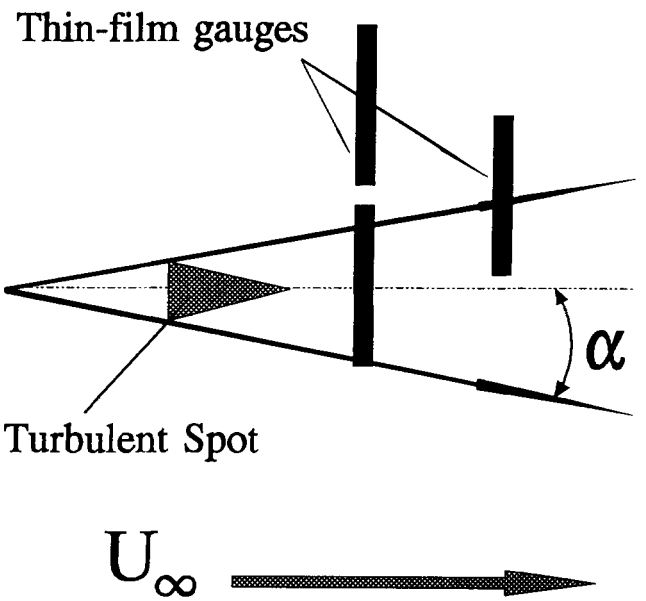

Fig. 9(b). A representation of the spreading of a single turbulent-spot over an array of thin-film gauges.

Experimental results

Figure 10 is a plot of turbulent-spot trajectories at conditions of zero pressure gradient, a gas-to-wall temperature ratio of 1.4, and a freestream Mach number of 0.55. Three trajectories are shown, and the fractional propagation rates associated with each line are

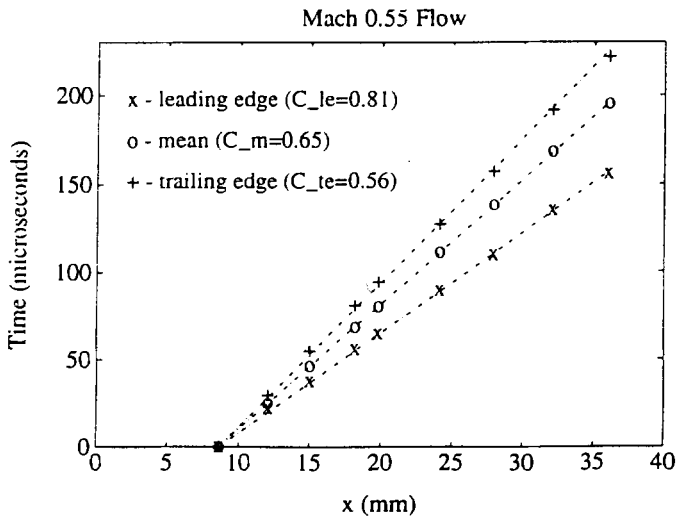

Fig. 10. Turbulent-spot leading-edge, trailing-edge, and "mean" trajectories for $M_\infty = 0.55$, $dP/dx = 0$, $Re_u = 7.5 \times 10^6/m$, $Tu = 0.1\%$, $T_0/T_w = 1.4$, and $z = 0mm$.

indicated. A weighted least-squares fit to the data points has been performed for each line, and the uncertainty in the individual measurements is within the height of the symbols on the plot. The "mean" trajectory was determined from cross-correlating the raw signals as described in Clark et al. [25]. Figure 11 is a plot of spot trajectories for the same conditions as those above except that the freestream Mach number is 1.86. Interestingly, the leading-edge, trailing-edge, and "mean" convection rates are nearly the same fraction of the freestream velocity for the Mach 0.55 and 1.86 cases. Also, the results agree very well with those of Schubauer and Klebanoff [3] for artificially-generated turbulent-spot leading- and trailing-edge convection velocities at incompressible conditions. It should be noted that this marks the first time that these parameters have been determined in "natural" transition at subsonic compressible and supersonic Mach numbers. The fractional propagation rates of the spots under four different Mach number flows are listed in Table 1.

In addition to the constant Mach number studies described above, experiments have been performed over a range of pressure gradients. Figure 12 is a plot of the variation of static-to-total pressure ratio with distance along the model surface for two of the convergent-divergent nozzles tested in this study, while Figure 13 is a plot of the local acceleration parameter (K) versus the same distance for the same nozzles. It can be seen in Figure 12 that both pressure gradients are zero for some 25 mm from the leading edge of the flat plate, at which point they become favourable, reaching constant values at roughly 45 mm from the leading-edge. For these nozzles, the inlet Reynolds numbers of the flow were set such that turbulent-spots were observed to form in the zero-pressure-gradient regions of the plate and then tracked as they were accelerated downstream.

There are some differences between the turbulent-spot trajectories measured in a zero-

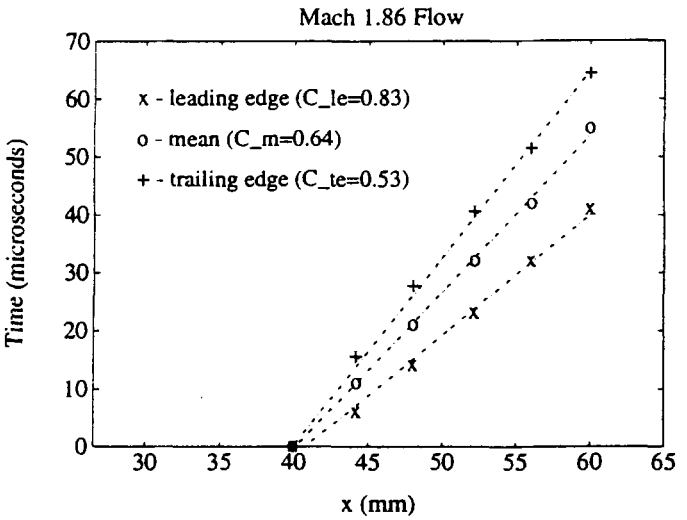

Fig. 11. Turbulent-spot leading-edge, trailing-edge, and "mean" trajectories for $M_\infty = 1.86$, $dP/dx = 0$, $Re_u = 16 \times 10^6/m$, $Tu = 0.1\%$, $T_0/T_w = 1.4$, and $z = 0mm$.

Table 1. Turbulent-spot fractional propagation rates at various freestream Mach numbers.

M_∞	C_{le}	C_{te}	C_m
0.24	0.86 ± 0.01	0.56 ± 0.01	0.65 ± 0.01
0.55	0.81 ± 0.01	0.56 ± 0.01	0.65 ± 0.01
1.32	0.85 ± 0.03	0.54 ± 0.01	0.64 ± 0.01
1.86	0.83 ± 0.04	0.53 ± 0.02	0.64 ± 0.02

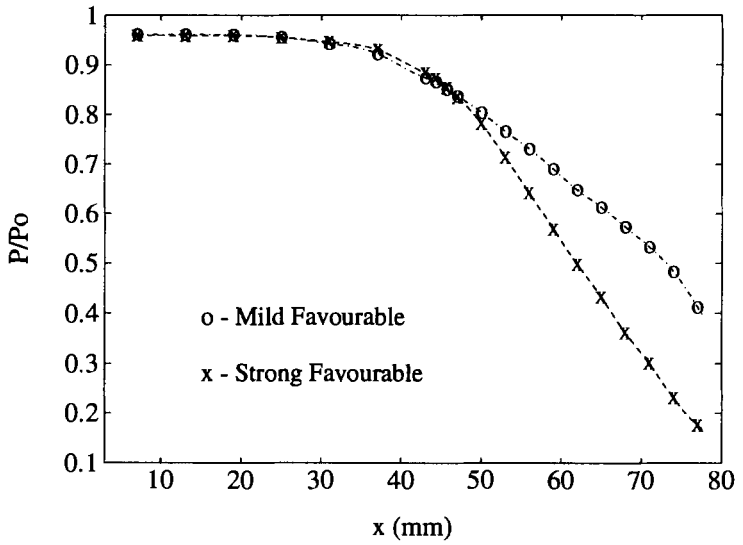

Fig. 12. Favourable pressure gradients which were studied.

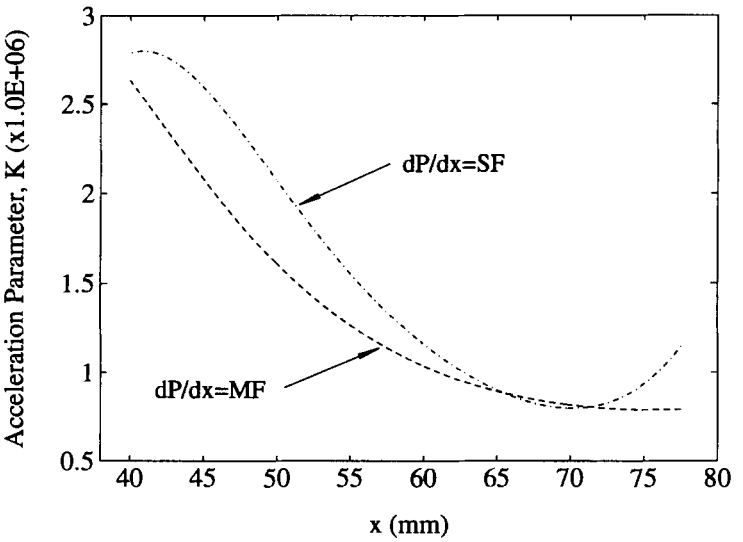

Fig. 13. The variation of the acceleration parameter, K, with distance along the flat-plate surface for the two pressure gradients studied.

pressure-gradient flow and the favourable pressure gradients described above. Figure 14 is a set of turbulent-spot trajectories for the mild-favourable pressure gradient case over the region where the pressure gradient is roughly constant (see Figure 12). For comparison, three lines of constant fractional propagation rate are plotted as well. It is evident that, over this region, the leading-edge velocity is a roughly constant fraction of the local freestream velocity and that this fraction is approximately equal to 0.9. However, the trailing-edge and "mean" convection rates do not scale directly with the local freestream velocity. Wygnanski [8] found that neither the leading- nor the trailing-edge velocity was proportional to that of the freestream in a favourable pressure gradient. The results of Wygnanski [8] have been interpreted by other researchers (Narasimha [26]) as implying that a turbulent spot has "memory" of its conditions at formation and is unaffected by subsequent increases in

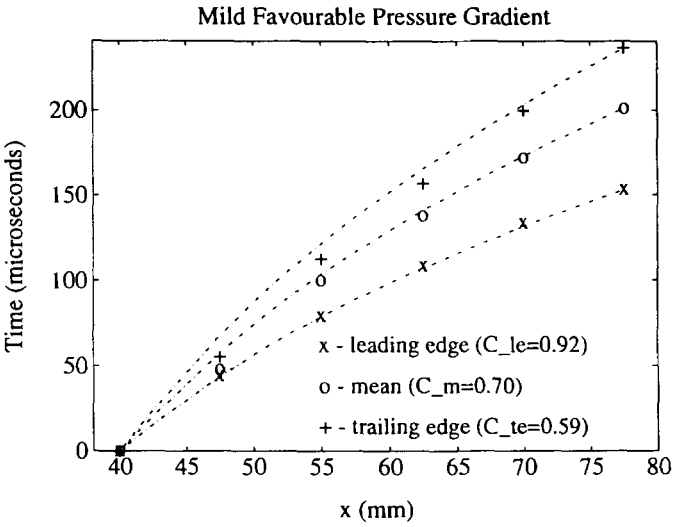

Fig. 14. Turbulent-spot leading-edge, trailing-edge, and "mean" trajectories for the mild favourable pressure gradient ($Re_u = 12 \times 10^6/m$, $T_0/T_w = 1.4$, $Tu = 0.1\%$, $z = 0mm$).

freestream velocity. No evidence of this latter effect is manifest in the results of this experiment. However, the current results are more in agreement with those of Sankaran and Antonia [10]. They found that, in a mildly-favourable pressure gradient, the leading-edge convection rate of the spot maintained the constant fraction of the local freestream velocity it normally takes under zero pressure gradient, while the propagation rate of the trailing-edge (as a fraction of U_∞) increased over its zero-pressure-gradient value.

It should be pointed out that there are differences between this experiment and the others discussed here [8, 10] which must be critical to the results. First, neither experiment [8,10] focused on a constant pressure gradient like those of this study. Second, in neither of the other experiments were turbulent spots tracked at acceleration parameters as high as those reported here (see Figure 13). Indeed, consideration of the effect of acceleration parameter on the fractional propagation rate of the trailing edges (C_{te}) of the spots proves instructive. If C_{te} is assumed to be constant over the interval between two successive thin films, then it can be represented by the equation

$$C_{te} = \frac{1}{\Delta t} \int_{x_1}^{x_2} \frac{dx}{U_\infty(x)}, \tag{7}$$

where Δt is the time of travel between the gauges located at x_1 and x_2, and U_∞ is the local freestream velocity.

In Figure 15, C_{te} is plotted versus the average acceleration parameter over the interval between the thin-film gauges, K. Data from both the mild favourable and strong favourable pressure gradients are shown, and the uncertainties of the measurements are indicated. For comparison, the fractional propagation rate of the leading edges of the spots over the same interval has been drawn as has the value of C_{te} in zero-pressure-gradient flow. It seems that at these conditions ($dP/dx = \text{constant}$) C_{te} is dependent on the value of the prevailing acceleration parameter. As K increases past 1×10^{-6}, C_{te} deviates from the value it takes in zero-pressure-gradient flow and begins to approach the fractional propagation rate of the leading edge. This implies a reduction in the streamwise growth rate of the spot, and this

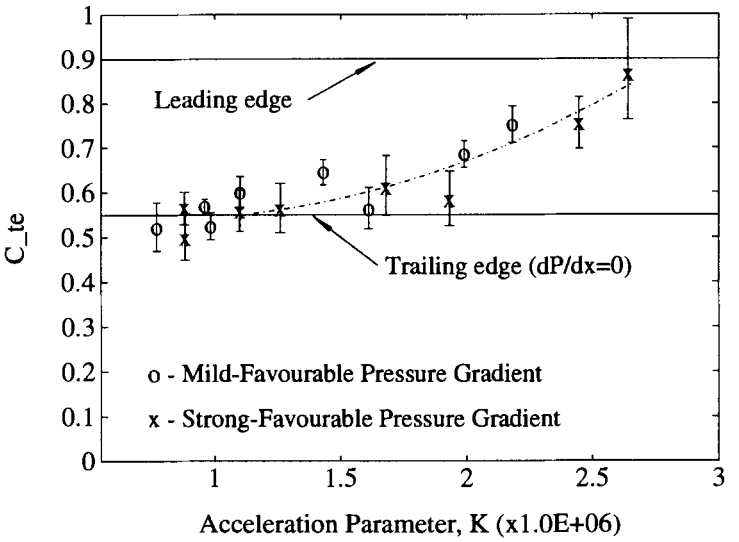

Fig. 15. The variation of the fractional propagation rate of the trailing edges of the spots with acceleration parameter for the two pressure gradients ($Re_u = 12 \times 10^6/m$, $T_0/T_w = 1.4$, $Tu = 0.1\%$, $z = 0mm$).

makes sense intuitively when one keeps in mind that a turbulent boundary layer will relaminarize if K reaches a certain threshold level ($\approx 3 \times 10^{-6}$).

Some results of turbulent-spot spreading angle at various conditions are presented in Table 2. It can be seen that, as expected, the lateral growth of turbulent spots is greatly inhibited by a favourable pressure gradient. This is in general agreement with estimates of the effect of pressure gradient from artificial-spot studies, and it supports the conclusions of Gad-el-Hak et al. [11] that spots spread laterally by the local destabilization of the laminar boundary layer at their edges. Also, the values of 8.2° and 6.0° given for the spreading angle at Mach numbers of 0.55 and 1.32, respectively, are significantly lower than that generally accepted at incompressible Mach numbers ($\approx$11° from Ref. 2) and indeed lower than the number deduced for the half angle at $M_\infty = 0.24$ in the current study. These results support the theoretical prediction of Doorly and Smith [27] that the spreading angle of a turbulent spot decreases monotonically as freestream Mach number increases. It should be pointed out that spreading angle has been found to be a weak function of the local Reynolds number by a number of researchers (e.g. Schubauer and Klebanoff [3] and Wygnanski [8]). However, the values reported for the subsonic Mach numbers were determined at equivalent values of Re_θ. The spreading angle at Mach 1.32 was obtained at a slightly higher value of Re_θ. Thus, the reported value at Mach 1.32 is if anything slightly larger than that which might have been found if complete equivalency of Re_θ had been obtained among all three cases.

Detailed results of turbulent-spot spreading-angle measurement in the favourable pressure gradients can be seen in Figure 16, which is a plot of the spot trajectory in the x-z plane. On

Table 2. Estimates of turbulent-spot spreading angles under various conditions.

Pressure gradient	Spreading Angle	Uncertainty
Zero, $M_\infty = 0.24$	9.9°	1.0°
Zero, $M_\infty = 0.55$	8.2°	0.8°
Zero, $M_\infty = 1.32$	6.0°	1.5°
Mild Favourable	3.9°	0.1°
Strong Favourable	3.3°	0.1°

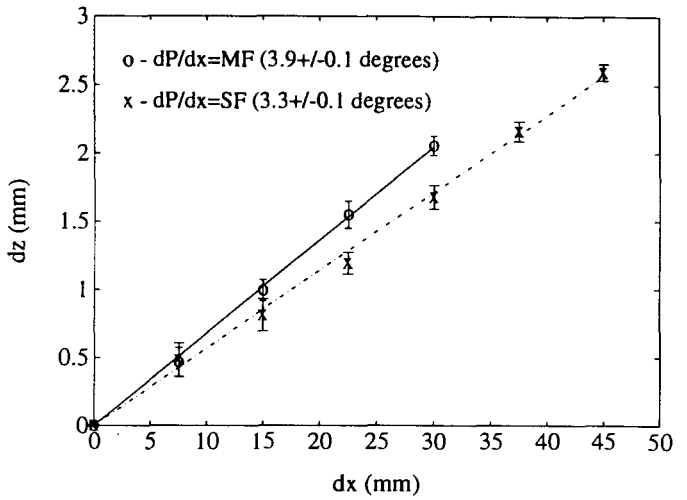

Fig. 16. Turbulent-spot lateral spreading under the influence of the favourable pressure gradients ($Re_u = 12 \times 10^6/m$, $T_0/T_w = 1.4$, $Tu = 0.1\%$). In the case of the mild favourable pressure gradient, $dx = x\text{-}50mm$, while $dx = x\text{-}35mm$ for the strong favourable.

Figure 16, the error bars denote the standard deviation of the results, and the trajectories have been measured over roughly the same intervals as those in the *x-t* plane. In contrast to the results of turbulent-spot growth in the streamwise direction (i.e. leading-edge and trailing-edge velocities), there appears to be no significant variation of turbulent-spot lateral growth (i.e. the slope of Figure 16 is constant) with the acceleration parameter, K. Again, note that the range of Figure 16 is that portion of the plate where the pressure gradient is constant (see Figure 12) and the acceleration parameter varies as illustrated in Figure 13.

Conclusions

Turbulent spots have been tracked in a boundary layer undergoing natural transition at gas-turbine-representative conditions. The separate effects of pressure gradient and compressibility on the growth characteristics of turbulent spots have been assessed. For the first time, turbulent-spot leading- and trailing-edge convection velocities have been extracted from natural-transition data at compressible conditions. It was observed that in a zero pressure gradient, the spot leading and trailing edges propagated at essentially the same fraction of the freestream velocity observed by other researchers at incompressible conditions. The constant favourable pressure gradients studied here were found to have little effect on the convection rate of the spot leading edges, which was found to be roughly the same fraction of the local freestream velocity seen in zero pressure gradient. By contrast, it was observed that the velocity of turbulent-spot trailing-edge propagation does not scale directly with that of the freestream and is dependent on the acceleration parameter.

It is also possible to make estimates of the growth rates of turbulent spots from the results of these experiments. Results of turbulent-spot spreading angles indicate that the lateral growth of turbulent spots is decreased by both favourable pressure gradients and increasing freestream Mach numbers. In addition, it was also shown that the streamwise growth of turbulent spots can be affected by a favourable pressure gradient. At large values of the

acceleration parameter, K, the trailing-edges of turbulent spots appear to propagate at rates which approach those of the spot leading-edges, implying a significant reduction of spot growth in the streamwise direction.

Acknowledgements

The advice of Dr. Patrick J. Magari during his tenure in the Oxford University Turbomachinery Group is greatly appreciated. Also, special thanks must go to Trevor Godfrey for his assistance in designing the working section of the tunnel and technical support throughout the study. Additional technical support was given by Leo Verling, and is greatly appreciated. Also, the advice of David Ashworth, of Rolls-Royce, plc., during the experimental program is greatly appreciated. In addition, thanks are due again to Dr. Patrick Magari as well as Albert J. Hofeldt, and Cyril Band for help in the production of the nickel thin-film-gauge array used in this study. Special thanks also to S.R. Smelser for assistance in the production of some of the figures in this report. The work herein was supported by the United States Air Force Office of Scientific Research under grant numbers F49620-92-J-0079 and 89-0427, with Major Daniel Fant acting as a technical monitor.

References

1. H.W. Emmons, The laminar-turbuent transition in a boundary layer-part 1. *Journal of Aeronautical Sciences* 18 (1951) 490–498.
2. J.J. Riley and M. Gad-el-Hak, The dynamics of turbulent spots. In: *Frontiers in Fluid Mechanics*. Berlin: Springer-Verlag Publishers (1985) pp. 123–155.
3. G.B. Schubauer and P.S. Klebanoff, Contributions on the mechanics of boundary layer transition. NACA TN-3489 (1956).
4. O. Savas, *Some measurements in synthetic turbulent boundary layers*. Ph.D. Thesis, California Institute of Technology (1979).
5. B. Cantwell, D. Coles, and P. Dimotakis, Structure and entrainment in the plane of symmetry of a turbulent spot. *Journal of Fluid Mechanics* 87 (1978) 641–672.
6. I. Wygnanski, M. Sokolov, and D. Friedman, On a turbulent 'spot' in a laminar boundary layer. *Journal of Fluid Mechanics* 78 (1976) 785–819.
7. T.S. Mautner and C.W. Van Atta, Wall shear stress measurements in the plane of symmetry of a turbulent spot. *Experiments in Fluids* 4 (1986) 153–162.
8. I. Wygnanski, The effects of Reynolds number and pressure gradients on the transitional spot in a laminar boundary layer. In: J. Jimenez (ed.) *Lecture Notes in Physics*. Berlin: Springer-Verlag Publishers 136 (1981) pp. 304–322.
9. Y. Katz, A. Seifert, and I. Wygnanski, On the evolution of a turbulent spot in a laminar boundary layer with a favourable pressure gradient. *Journal of Fluid Mechanics* 221 No. 12 (1990) 1–22.
10. R. Sankaran and R.A. Antonia, Influence of a favourable pressure gradient on the growth of a turbulent spot. *AIAA Journal* 26 No. 7 (1988) 885–887.
11. M. Gad-el-Hak, R.F. Blackwelder, and J.J. Riley, On the growth of turbulent regions in laminar boundary layers. *Journal of Fluid Mechanics* 110 (1981) 73–95.
12. T. Matsui, Visualization of turbulent spots in the boundary layer along a flat plate in a water flow. In: R. Eppler and H. Fasel (eds.) *Laminar-Turbulent Transition*. Berlin: Springer-Verlag Publishers (1980) pp. 288–296.
13. D.L. Schultz and B.J. Bellhouse, Determination of mean and dynamic skin friction, separation, and transition in low-speed flow with a thin-film heated element. *Journal of Fluid Mechanics* 24 (1966) 379–400.
14. F.K. Owen, Transition experiments on a flat plate at subsonic and supersonic speeds. *AIAA Journal* 8 No. 3 (1970) 518–523.
15. D.J. Doorly, M.L.G. Oldfield, and C.T.J. Scrivener, Wake-passing in a turbine rotor cascade. In: *Heat Transfer and Cooling in Gas-Turbine Engines*. Agard CP-390 (1985) Paper No. 7.

16. J.E. LaGraff, D.A. Ashworth, and D.L. Schultz, Measurement and modelling of the gas turbine transition process as disturbed by wakes. *ASME Journal of Turbomachinery* 111 (1989) 162–168.
17. R.P. Shiply, N.T. Birch, H. Riedel, K.H. Horstmann, and P. Lücking, A European Collaborative NLF Nacelle Flight Demonstrator. In: *Proceedings of the 1st European Forum on Laminar-Flow Technology*. Hamburg: (1992). Also In: *Aviation Week and Space Technology* 21 No. 12 (1992).
18. N. Bown, T.M. Cain, P.J. Magari, and T.V. Jones, Analysis of NLF testing. Oxford University O.U.E.L. Report (1993).
19. T.V. Jones, D.L. Schultz, and A.D. Hendley, On the flow in an isentropic light piston tunnel. *ARC 34217* (1973).
20. J.P. Clark, P.J. Magari, T.V. Jones, and J.E. LaGraff, Experimental studies of turbulent-spot parameters using thin-film heat-transfer gauges. *AIAA Paper No. 93–0544* (1993).
21. D.L. Schultz and T.V. Jones, Heat transfer measurements in short-duration hypersonic facilities. *NATO Agardograph 165* (1973).
22. M.L.G. Oldfield, H.J. Burd, and N.G. Doe, Design of wide-bandwidth analogue circuits for heat-transfer instrumentation in transient tunnels. In: *Proceedings of the 16th Symposium of ICHMT*. Dubrovnik: Hemisphere Publications (1982).
23. R. Narasimha, The laminar-turbulent transition zone in the boundary layer. *Progress in Aerospace Sciences* 22 (1985) 29–80.
24. T.B. Hedley and J.F. Keffer, Turbulent/non-turbulent decisions in an intermittent flow. *Journal of Fluid Mechanics* 64 (1974) 645–678.
25. J.P. Clark, T.V. Jones, D.A. Ashworth, and J.E. LaGraff, Turbulent-spot development in a Mach 0.55 flow. In: *Proceedings of the Royal Aeronautical Society Boundary Layer Transition and Control Conference* (1991) Paper No. 21.
26. R. Narasimha, Recent advances in the dynamics of the transition zone. *ISABE Paper No. 91–7006* (1991).
27. D.J. Doorly and F.T. Smith, Initial-value problems for spot disturbances in incompressible and compressible boundary layers. *Journal of Engineering Mathematics* 26 (1992).